

Ion Impregnation Effect of Fe, Cu, Cr-attributed Mordenite on Stearic Acid Cracking

Abdulloh Abdulloh, Ulfa Rahmah, Satya Candra Wibawa Sakti, Alfa Akustia Widati, Ahmadi Jaya Permana, Rochadi Prasetya, Musbahu Adam Ahmad, and Mochamad Zakki Fahmi*

Department of Chemistry, Faculty of Science and Technology, Airlangga University, Surabaya 60115, Indonesia

* **Corresponding author:**

email: m.zakki.fahmi@fst.unair.ac.id

Received: December 10, 2021

Accepted: March 28, 2022

DOI: 10.22146/ijc.71126

Abstract: The improvement in the design of mordenite-based catalysts focuses on the present study to fulfill the massive demand for bio-aviation fuel (BAF) as renewable energy. Modification of the mordenite through ionic impregnation of Fe, Cu, and Cr, has supported the mordenite to perform with better efficiency and activity in catalyzing the cracking process of stearic acid. The adjustment on catalytic activity was carried out by simply reacting the catalyst with stearic acid at 190 °C and investigating cracking products with Gas Chromatography-Mass Spectroscopy. The results of the GC-MS test of the cracking product showed the formation of alkane-alkene and aromatic compounds. BAF was selectively obtained (30.27%) when the reaction was catalyzed by FeCuCr/mordenite catalyst. The BAF derived from FeCuCr/mordenite contained hydrocarbons that include xylene, mesitylene, dodecane, tridecane, tetradecane, and pentadecane. However, reduced selectivity was realized (19.85%) when the reaction was catalyzed by nano FeCuCr/mordenite. Its hydrocarbon constituents include benzene, tetradecane, and pentadecane compounds.

Keywords: mordenite; stearic acid; metal impregnation; cracking

■ INTRODUCTION

The massive development of transportation technology increases the need for fuel that mostly comes from unrenovable oil sources. This condition emerges the need for an alternative source to reduce such problems by using renewable materials, such as BAF and biodiesel. Blakey et al. explained that aviation fuel is a hydrocarbon with a range of carbon chains C₈-C₁₆ [1]. The hydrocarbon component in aviation fuel consists of paraffin (alkane), naphthalene (alkenes), cycloparaffine (cycloalkanes), and/or aromatic hydrocarbon. Sabarman et al. produced aviation fuel compounds from palm fatty acid distillate (PFAD) through hydrotreating and hydrocracking. All these methods were catalyzed by NiMo/ γ -Al₂O₃ catalyst at a temperature of 400 °C. In this study, the production of hydrocarbons with high C₁₅ carbon chains was reported. The production was influenced significantly by 3% (wt.%) catalyst loading [2]. Also, other catalysts based on Ni-Mo/SiO₂ and NiMo/zeolite were also reported to increase BAF production and activity [3-4]. In the case of zeolite

application, Carli et al. reported the synthesis of aviation fuel from oleic acid through hydrodeoxygenation reaction of NiMo/zeolite at temperature and pressure conditions were 375 °C and 15 bar, respectively. The catalyst results in the production the aviation fuel, whose yield was up to 36.32% for a 2.5 h reaction time [4]. The above reports indicated that the compounds of aviation fuel could be produced from fatty acid-based compounds, and zeolite can contribute to the reaction as a supported catalyst.

Well-known as an excellent and suitable material as a catalyst, zeolite showed excellent properties, such as stability at high temperatures, good activity, microporous, and high acid sites. The industries, as well as other researchers, preferred using heterogeneous catalysts because they are less prone to multi-step neutralization and also due to their economic advantages [5-6]. The first aspect is the crystallinity of the zeolite, which can affect the catalytic activity [7]. Besides the crystallinity, the acid sites and zeolite pore also determine its performance. The last two factors are

quite crucial in setting a good catalyst and allowing researchers to do modifications by increasing the acid site or restructuring the zeolite to get high porosity on it. To get the acid site strengthened, the catalyst could be modified by adding a metal element that would possibly enhance the activity of the catalyst [5]. The cationic metals can serve as Lewis acid sites. This site will capture H atoms from hydrogen gas which will be transferred to hydrocarbon compounds that have been cracked by Bronsted acid sites on the catalyst [8]. Therefore, this study proposes the application of modified mordenite to produce Aviation fuel from stearic acid. Stearic acid is a common compound found in vegetable oils. It can be found in palm oil coarse (CPO) by 5% [9], 35% in brown [10], 4.9–8.6% in kapok seed oil [11], and 12.66% in the seeds of the rubber [12]. In animal sources, stearic acid can also be found in beef fat as much as 20–25%, pork fat at 12–16% [13], and chicken fat at 17.55% [14].

The importance of metals in modifying new properties of mordenite is interesting to be explored. Some studies proposed the addition of metal by chemical interaction with mordenite support to make the struggle mode of the catalyst. One of the chemical interactions is impregnation. The impregnation method is the most advantageous as it maximizes the use of the active component with the lowest dosage [15]. The impregnation of Ni to HZSM-5/SBA resulted in a bimodal structure and demonstrated efficient performance capable of producing 40% aromatics and 80% cyclic hydrocarbons conversion products, which are important components of jet fuel [16]. Impregnation of trimethyl phosphate on HZSM-5 nano zeolite was able to increase hydrothermal stability so that there was an increase in catalytic performance in the conversion of olefin into gasoline [17]. Impregnation of CuCo catalyst with carbon nanotubes (CNT) was successfully synthesized and could convert stearic acid into biodiesel with a selectivity of 94.82% [18]. Impregnation of Ni into the HZSM-5 catalyst was made by immersing HZSM-5 in a solution of nickel nitrate ($\text{Ni}(\text{NO}_3)_2$), which resulted in the enhanced catalytic performance of the catalysts in trimerization of *n*-butane [19]. Catalytic conversion of methanol to valuable products like *p*-Xylene impregnated with zinc

[20–21]. Impregnation can reduce BAS (Brønsted acid sites) and increase LAS (Lewis acid sites) in the pores of the zeolite [21]. This property, coupled with appropriate reaction conditions, resulted in an increase in selective conversion to *p*-Xylene [21]. The purpose of this method is to fill the pores of the support layer with a precursor solution containing a sufficient concentration of metal salts to achieve the desired loading [22]. Even though several studies also report the application of impregnation (physical binding) on introducing metal on the zeolite and it successfully obtains aviation fuel components from oleic acid compound [4]. However, the inclusion of metal on zeolite through impregnation to convert the fatty acid into aviation fuel has not been well explored previously. The present study will try to overcome the above gap by modifying raw mordenite (as zeolite class abundantly found in nature) from commercial cat sand with simple metal impregnation. Trimetallic catalysts made from transition metals are common [23]. Some metals such as iron (Fe), copper (Cu), and chromium (Cr) were also introduced to mordenite to support the cracking process of stearic acid in obtaining aviation fuel components. Besides the characterization of the catalyst, further observation is focused on evaluating selectivity towards obtaining aviation fuel compounds. The selectivity of producing alkane and the conversion percentage of stearic acid were also studied. Overall, the study investigated the effect of metal impregnation and catalyst size reduction on catalytic performance.

■ EXPERIMENTAL SECTION

Materials

The materials used in the present study consist of commercial cat sand purchased from a local market in Surabaya, Indonesia. Other chemicals such as Hydrofluoric Acid (HF, 40%), Hydrochloric Acid (HCl, 37%), Ammonium Chloride (NH_4Cl , 99%), Silver Nitrate (AgNO_3), Stearic Acid, Iron(III) Chloride Hexahydrate ($\text{FeCl}_3 \cdot 6\text{H}_2\text{O}$, 97%), Chromium(III) Chloride (CrCl_3 , 99%), and Copper(II) Chloride Dihydrate ($\text{CuCl}_2 \cdot 2\text{H}_2\text{O}$, 99%) were all purchased from Sigma Aldrich (St. Louise, USA). Ethanol and *n*-hexane as solvents were purchased

from Bratachem Ltd (Surabaya, Indonesia). All chemicals are used without particular purification.

Procedure

Preparation of catalyst

The catalyst preparation was done by following a number of stages. Firstly, the cat sand was soaked in a solution of HF 1% for 30 min to remove the non-framework silica (quartz-free) and washed with distilled water to reach neutral pH. Furthermore, the quartz-free mordenite was immersed in 6 M of HCl for 30 min at a temperature of 50 °C, followed by washing with distilled water. The obtained material was then submerged in NH₄Cl 1 N with a set temperature of 90 °C and stirred the mixture roughly for 3 h, followed by curing the mixture over seven days. The solid was then filtered and washed with distilled water to get Cl-free, then the sample was dried in an oven at a temperature of 110 °C for 3 h. Then, the obtained sample was sieved to a size of 140 mesh, and the solid obtained was called H-mordenite.

Secondly, impregnation of metal ions was done. Experimentally, the above-resulted sample was mixed with a 10% aqueous solution of CrCl₃ and refluxed at 50 °C for 30 min. The pH was set between a range of 10–12 following the addition of hydrazine (6 mL). This sample was then washed with flowing distilled water to get a Cl-free sample and dried at 110 °C for 24 h. It continued by calcining at 500 °C for 5 h with nitrogen flow. The obtained product was marked as Cr/mordenite. This protocol was repeated by changing the Cr source with Fe and Cu to produce the other ion-modified mordenite. Thirdly, the size of the catalyst was reduced. Experimentally, the impregnated mordenite (25 g) was added to agate jars and treated on a ball-milling machine BKBM-V2S (Biobase, China) at 300 rpm for 5 h. The mordenite with reduced size was subsequently used to catalyze the cracking of the stearic acid.

The activity of the catalyst

The cracking reaction of stearic acid is mediated on a fractional distillation set, including a fractionation column, condenser, and thermocouple. The FeCuCr/mordenite and stearic acid (1:50) are inserted into the reaction flask and heated at 190 °C to initiate a

cracking reaction (under a vacuum condition). After a reaction proceeded, at adjusted times, about 0.1 mL of the product was collected and dissolved in 10 mL of *n* hexane-ethanol mixture (1:1). At the end of the cracking process, the catalyst was collected and separated from the liquid phase by centrifugation. The conversion of stearic acid and selectivity to BAF were calculated based on the following equations:

$$\text{Stearic acid conversion (\%)} = 100\% - \% \text{ stearic acid area}$$

$$\text{BAF Selectivity (\%)} = \frac{\text{bioavtur area}}{\text{stearic acid converted}} \times 100\%$$

Characterizations

Several instruments were used to characterize the catalyst, including X-ray Diffraction (XRD) Phillips Analytical JOEL JDX-3530, X-ray Fluorescence (XRF) PANalytical Epsilon 4, Scanning Electron Microscopy (SEM) Zeiss Evo 40 Series, and Fourier Transform Infrared (FTIR) Shimadzu 84005. Characterization for the resulting BAF was confirmed by Gas Chromatography-Mass Spectrometry (GC-MS) Agilent GCMS 5977B.

X-ray diffraction analysis was carried out using a solid powder sample placed on a glass plate and analyzed with Cu K α radiation ($\lambda = 1.5405 \text{ \AA}$) at 2θ between 10°–80°. The results obtained are in the form of diffractogram peaks, and from these peaks, a material can be identified as having a crystal structure or not.

Determination of the type and number of acid sites in the catalyst using the pyridine-FTIR method. The working process is that the sample is heated at 400 °C for 2 h and cooled and then put into a glass tube which has a place to drain N₂ gas and drip pyridine. Then it was put into a tubular furnace and heated at 150 °C for 30 min while N₂ gas was flowing. Then pyridine was added from the tube through the faucet, and N₂ gas was still flowing. After the pyridine liquid dries, the N₂ gas flow is closed, and the end of the tube is clamped. The sample was cooled at room temperature. Then the sample was tested for acid sites using FTIR at a wavenumber of 1540–1545 cm⁻¹, indicating the presence of a Brønsted acid site, and at a wavenumber of 1440–1452 cm⁻¹, indicating the presence of a Lewis acid site. The number of the acid side of Brønsted and Lewis can be calculated based on the following equation [25]:

$$C_L = \frac{\pi}{\text{IMEGC}_L} \times \frac{r^2}{w} \times A_{1450} \quad (1)$$

$$C_B = \frac{\pi}{\text{IMEC}_B} \times \frac{r^2}{w} \times A_{1540} \quad (2)$$

where C_L and C_B are the concentration of Lewis (L) and Brønsted (B) acid sites in mmol g^{-1} ; A_{1450} and A_{1540} are integrated areas of bands at 1450 and 1540 cm^{-1} ; IMEC_L and IMEC_B are molar extinction coefficients of 2.22 and 1.67 $\text{cm } \mu\text{mol}^{-1}$, respectively. The r value refers to pellet radius in cm, and w is the pellet weight in mg.

In the morphological assessment by SEM method, the sample is inserted into a brass stub sample holder using a double stick carbon tape, then sputtered with Au for 15 min, with a pressure of 6×10^2 mBar. Next, the sample holder is placed on the instrument, and an analysis is carried out.

Observation of the composition of the catalyst was measured using the direct exposure of powder solids to X-ray Fluorescence (XRF). The analysis was carried out with the sample that had been finely inserted into the sample tube and pressed until the surface was flat. Then placed in the instrument and analyzed.

RESULTS AND DISCUSSION

FeCuCr/Mordenite

The catalysts that were successfully synthesized were then characterized using X-ray Diffraction (XRD), X-ray Fluorescence (XRF), Scanning Electron Microscopy (SEM), and Fourier Transform Infrared (FTIR). The characterization of the resulting BAF was confirmed by Gas Chromatography-Mass Spectrometry (GC-MS).

The XRD was firstly carried out to observe the crystal structure of the obtained zeolite. From Fig. 1, it can be seen that there is a similarity in the peak of bare mordenite with other modified mordenites even though there are some additional peaks. The diffractogram changes could be observed by the appearance of new peaks and the change of d-spacing. The XRD diffractogram of the bare mordenite was confirmed by X'Pert HighScore (JCPDS #01-073-1490), where it showed particular peaks with 2θ at 20.79, 22.19, 25.52, 26.56, 27.72, and 35.58°; whereas H-mordenite showed peaks at 2θ of 20.78, 22.20, 25.60, 26.53, 27.66, and 36.45°. The results clarify the

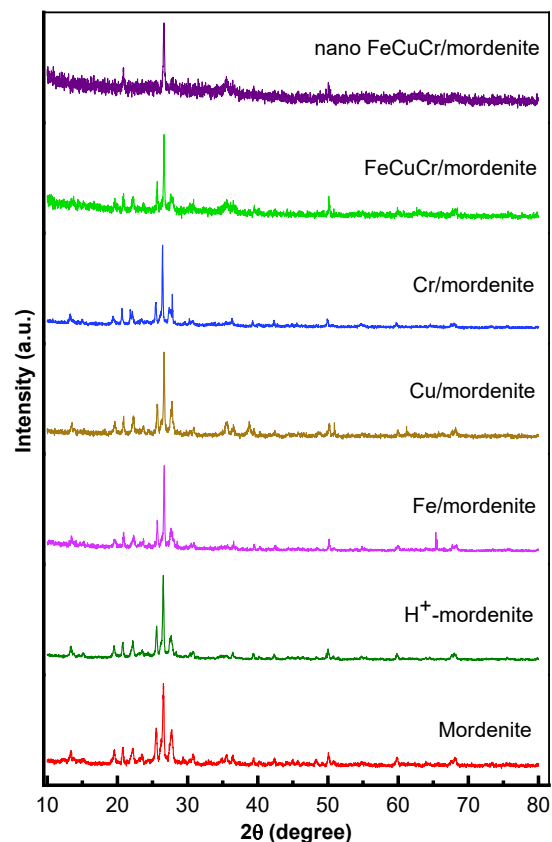


Fig 1. XRD patterns of mordenite, H-mordenite, Fe/mordenite, Cu/mordenite, Cr/mordenite, and FeCuCr/mordenite

the diffractogram of H-mordenite has not undergone significant changes compared with bare mordenite because the peaks on the bare mordenite re-emerged on the H-mordenite pattern. The d-spacing comparison of both samples also does not make a difference much. However, the quartz composition decreased from 10.6% (in mordenite) to 8.5% (in H-mordenite). This indicates that after HF and HCl treatment, silica-free mordenite was obtained.

Further impregnation of metals into the mordenite with varied metal combinations affected the diffractogram, however, each sample still maintains the crystalline structure by performing sharp peak patterns. In particular, the diffractogram pattern of Fe/mordenite has peaks at 2θ values of 20.87, 22.31, 25.68, 26.65, 27.64, and 36.55°. The peaks have relative intensities of 17.93, 14.25, 30.78, 100, 22.54, and 7.64%, which shows there is mordenite in the sample. The diffractogram of the

Cu/mordenite has a peak at 2θ values of 20.86, 22.29, 25.68, 26.64, 27.78, and 36.50°, and each has a relative intensity of 19.15, 18.95, 35.11, 100, 33.81, and 8.69%. The diffractogram of the Cr/mordenite in the 2θ region of 25°–28° has a relatively less intense peak compared to the H-mordenite. It smoothly indicates the crystallinity of Cr/mordenite was decreased. The results of three metal combination mordenite showed its similarity with bare mordenite, which indicated the existing mordenite phase in the samples. The d-spacing comparison on the Cr/mordenite on the peak area of 9.49, 19.37, and 22.10° shifts the peak to the right. This shifting indicated that metal ion impregnation into the mordenite was successful. The diffractogram of FeCuCr/mordenite owing 2θ peaks at 20.86, 26.63, and 35.54° with relative intensities of 15.38, 100, and 9.44%, respectively, which indicated the existence of individual mordenite in the sample. The diffractogram of nano FeCuCr/mordenite showed a peak at 2θ values of 20.86, 26.62, and 35.48° with relative intensities of 23.12, 100, and 10.92%, thus, also indicating the existence of mordenite in the sample. The increased intensity indicates that the nano-sized FeCuCr/mordenite was more crystalline when compared to FeCuCr/mordenite. The XRD showed the impregnation of 3 metals into mordenite, which resulted in the loss of some peaks at around $2\theta = 13.45^\circ$. The peak around $2\theta = 26.62^\circ$ did not reappear in the nano FeCuCr/mordenite. The peak intensity of grinded-

FeCuCr/mordenite was lower than FeCuCr/mordenite, while increased noise peaks were observed on the diffractogram of nano FeCuCr/mordenite. This observation showed the influence of the grinding process on FeCuCr/mordenite. The lower peak intensity could be attributed to the reduced size crystallites of mordenite due to the grinding process.

The X-ray Fluorescence technique was used to observe the elemental composition before and after the impregnation of metal in mordenite. Table 1 shows Fe element is not detected on both bare mordenite and H-mordenite due to the small amount of this element. Furthermore, the Fe signal increases drastically when the impregnation of H⁺-mordenite by Fe metal with a percentage up to 33.71%; and revealed the catalyst impregnation of Fe/mordenite was successfully prepared with the presented protocol. Similarly, the composition of the Cu and Cr that were initially absent on bare mordenite comes to a high percentage (up to 50.18 and 51.9%, respectively) after its impregnations. The impregnation of 10% metals in a ratio of (1:1:1) produces XRF data that corresponds to the percent composition of Fe:Cu:Cr (28.0%:22.8%:23.8%). In addition, there are also the elements that declined in the composition, namely K, Ca, and Ti, but are not completely gone after the impregnation. This result can be assumed that the metal was replaced by impregnating metals through substitution isomorphous. Thus, the data

Table 1. Elemental composition of mordenite, H-mordenite, Fe/mordenite, Cu/mordenite, Cr/mordenite, FeCuCr/mordenite, nano FeCuCr/mordenite

Composition (%)	Sample						
	Mordenite	H-mordenite	Fe/mordenite	Cu/mordenite	Cr/mordenite	FeCuCr/mordenite	Nano FeCuCr/mordenite
Al	8.80	6.60	6.98	0.30	4.03	2.50	-
Si	58.00	70.60	52.21	43.60	32.40	18.4	18.30
K	4.96	5.49	3.36	2.26	1.82	1.10	1.00
Ca	16.10	4.78	1.94	1.66	1.18	0.63	1.00
Ti	1.60	1.40	0.95	0.63	0.56	0.32	0.28
Fe	-	-	33.71	-	-	28.00	27.6
Cu	-	-	-	50.27	-	22.80	30.0
Cr	1.00	-	0.52	0.71	51.90	23.80	21.0
Mn	5.90	5.20	0.27	0.35	7.10	0.480	0.27

reveals a successful impregnation process of the metal on the zeolite. The Si/Al ratio in FeCuCr/mordenite was 7.36 and then increased in size, reducing FeCuCr/mordenite by 17.89. The Si/Al ratio is the ratio of the amount of silica to aluminum contained in the sample. The increase in the Si/Al ratio affects the reactivity and stability of the zeolite. A large number of Si/Al ratios can affect the acidity of mordenite, where the greater the ratio value, the higher the acidity.

Fig. 2 shows the FTIR spectra of the Fe/mordenite, Cu/mordenite, Cr/mordenite, FeCuCr/mordenite and nano FeCuCr/mordenite. The peaks at 787–799 cm^{-1} referred to the presence of vibrational bending of the T–O–H for the metal binding, whereas the vibrational stretching of Al–OH is on wavenumber 3590–3642 cm^{-1} . The peaks at 1057–1122 cm^{-1} showed the vibrational stretching of Si–O–Si, and the peaks at 1224–1231 cm^{-1} showed the vibrational stretching of Si–O–Al [24]. The peaks at 1622–1636 cm^{-1} indicate the presence of vibration of OH molecules of water, and peak vibration bending Si–O–Si or Si–O–Al appears in the wavenumber 460–480 cm^{-1} [25]. This data supports the above XRD and XRF data which claimed a successful metal impregnation on the zeolite.

Pyridine-FTIR method for determining the type and amount of acid sites in the obtained catalyst was carried out. In this protocol, the acid sites on the sample are banded at 1540–1545 cm^{-1} for Brønsted acid and 1440–1452 cm^{-1} for Lewis acid [26]. From the data, FeCuCr/mordenite catalyst emerges Brønsted acid site observed at wavenumbers 1546 cm^{-1} and Lewis acid site on the 1441 cm^{-1} . Moreover, nano FeCuCr/mordenite also presented Brønsted acid around 1547 and 1442 cm^{-1} for the Lewis acid (Fig. 3). After the calculation, the number of the Brønsted site on FeCuCr/mordenite and nano FeCuCr/mordenite were 964.36 and 1356.87 $\mu\text{mol g}^{-1}$, respectively. Then, the number of Lewis acid sites of FeCuCr/mordenite and size-reduced FeCuCr/mordenite were 213.65 and 249.33 $\mu\text{mol g}^{-1}$, respectively. The number of acid sites of nano FeCuCr/mordenite was found to be greater than that of FeCuCr/mordenite. These results revealed that decreasing the size of the catalyst will increase the number of acid sites. This leads to a resulted

increase in active surfaces on the catalyst, thus resulting in better catalytic ability. In addition, the number of Brønsted and Lewis acids was also affected by the ratio of Si/Al as informed by previous XRF data, thus, increasing of Si/Al ratio will promote the acidity of the Brønsted-Lewis.

SEM analysis of the modified catalyst is shown in Fig. 4. The morphology of bare mordenite (Fig. 4(a)) shows irregular granules as a common zeolite-based catalyst. Moreover, further size modification on size-reduced FeCuCr/mordenite results in more homogenous granules that tend to be smaller particles.

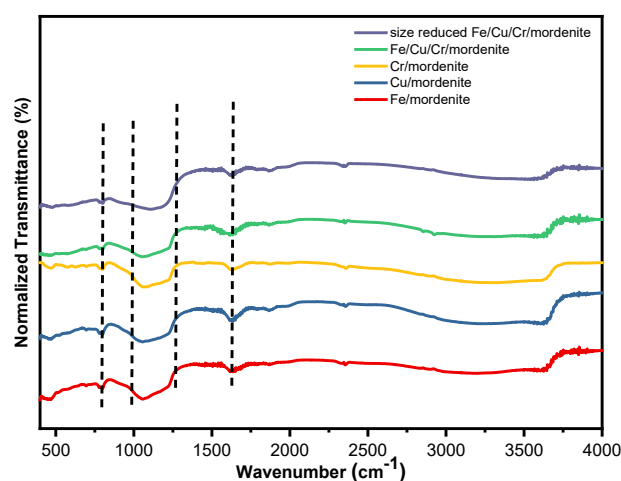


Fig 2. FTIR spectra of (a) Fe/mordenite, (b) Cu/mordenite, (c) Cr/mordenite, (d) FeCuCr/mordenite, and (e) Nano FeCuCr/mordenite

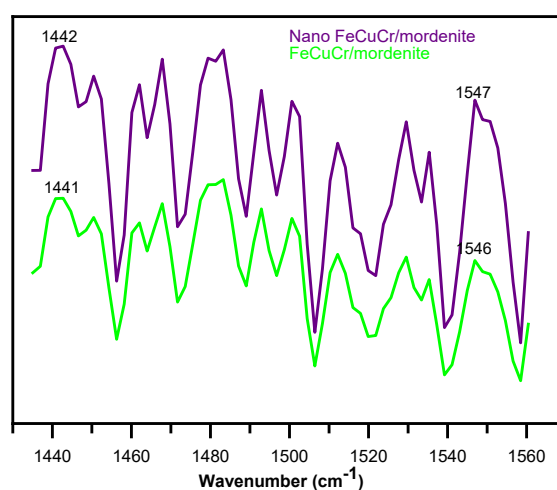


Fig 3. The acidity of FeCuCr/mordenite and Nano FeCuCr/mordenite

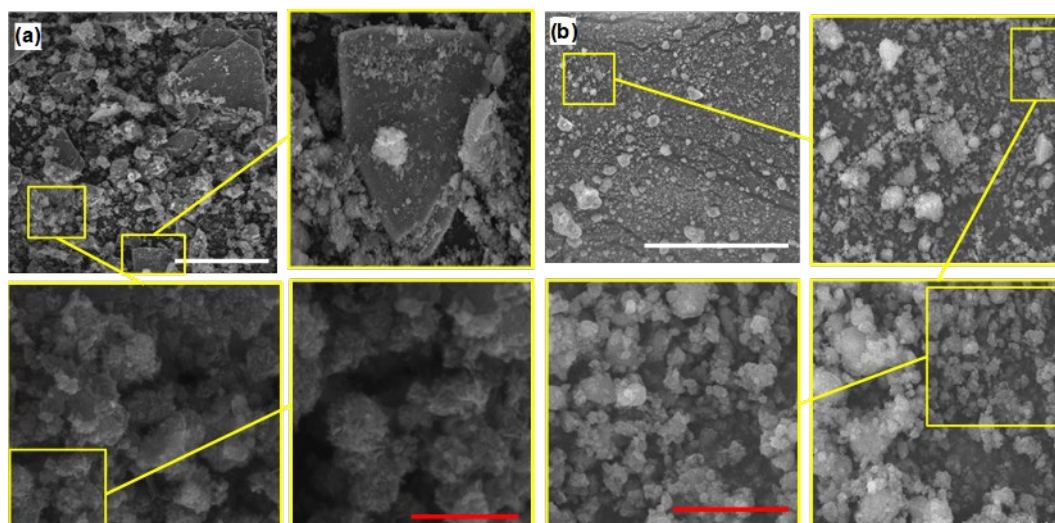


Fig 4. SEM images of (a) FeCuCr/mordenite and (b) size reduced FeCuCr/mordenite. The magnification of the adjusted area is indicated with yellow squares. White and red bars represent 100 μm and 2 μm , respectively

The result showed that the ball-milling process successfully decreased the diameter of the catalyst and increased acid sites, as previously discussed while describing pyridine-FTIR data.

Performance of the Catalyst

The chromatogram results of the sample after the cracking reaction for an initial 3 h showed the presence of

several formed compounds, namely alkanes, alkenes, alkynes, carboxylic acids, aromatic and other compounds (non-hydrocarbon) (Fig. 5). The formation of hydrocarbons (alkanes, alkenes, alkynes) through a decarboxylation reaction of stearic acid with the catalyst will produce heptadecane. A decarboxylation reaction that occurs mainly was affected by the Lewis acid site in

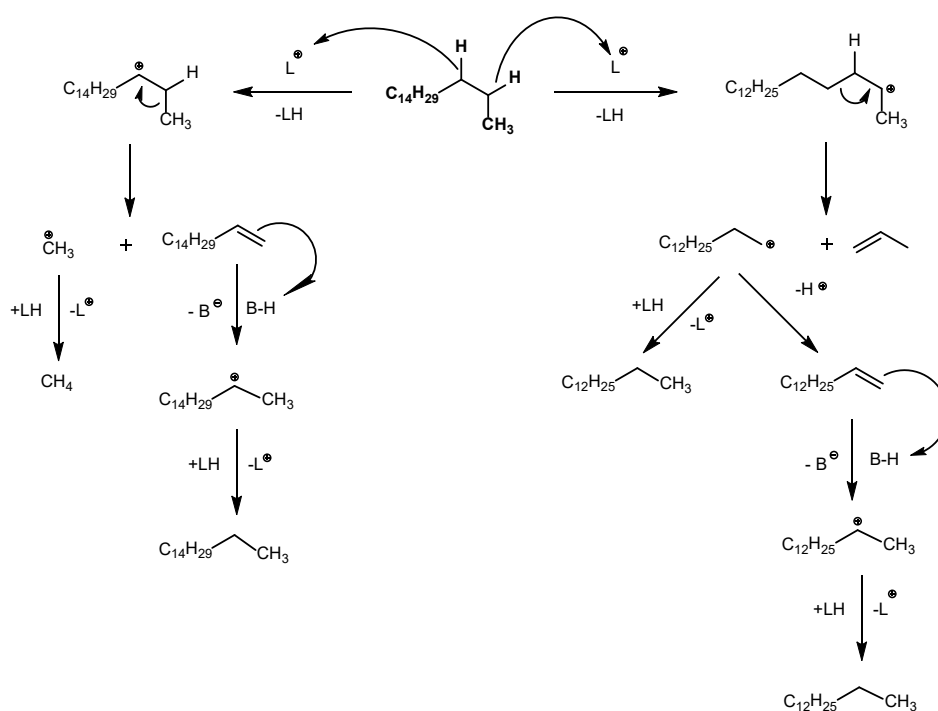


Fig 5. Mechanism of catalytic cracking reaction of heptadecane obtained from stearic acid decarboxylation reaction

the catalyst. It is thought that the oxygen attacks the Lewis acid sites on the carbonyl stearic acid, resulting in temporary binding. Subsequently, stearic acid rearranges ions, releasing the hydrogen ion. A carbon atom at the alpha (α) binding position of the hydrogen atoms obtains the heptadecane compound. This compound reacts with the acid sites again and lets the following cracking produce shorter hydrocarbon fragments (Fig. 5). Optimization of the catalytic process for producing aviation fuel components and alkane components through modification on single metal impregnation, combined metal impregnation, and size-reduced catalyst (Fig. 6–8). The cracking results of stearic acid with Fe/mordenite can be seen in Fig. 5. After the reaction for 0.5 h, 83.78% of stearic acid was converted, after 1 h up to 90.22% were converted, and after 2 to 3 h, stearic acid was completely converted to the product (Fig. 8). Method optimization for the selective production of aviation fuel by the Fe/Mordenite was done over a range of reaction times. After half an hour of the reaction time, 16.64% of the BAF was selectively produced. After 1 h, selectivity increased to 28.92%, while as high as 55.98% selective production was realized after 2 h. However, beyond 2 h of reaction time, a decrease in selectivity was observed. Therefore, it could be considered that the optimum time for the production of BAF by Fe/Mordenite catalyst is when the reaction is allowed to take place for 2 h. The components of the BAF were characterized and found to be hexadecane, pentadecane, tetradecane, tridecane, dodecane, undecane, decane, nonane, cyclohexadecane, cyclopentadecane, decylbenzene, nonylbenzene, and ethylbenzene. The Cu/mordenite catalyzed cracking of stearic acid to yield aviation fuel having the yield of 7.01, 7.16, 17.19, 30.56, 40.17, and 42.72% for 0.5, 1, 1.5, 2, 2.5, and 3 h, respectively (Fig. 6), the hydrocarbons that were produced as avtur compound are dodecane, pentadecane, and hexadecane. The conversion of stearic acid with Cr/mordenite also increased from 0.5 to 3 h, and the product components of aviation fuel also became higher (Fig. 6). The resulting fractions from Cr/mordenite catalysis included a BAF whose components are tridecane, (E)-2-tetradecane, tetradecane, 1-pentadecene, pentadecane, cetene, hexadecane, and decylbenzene. In Fig. 6, it was

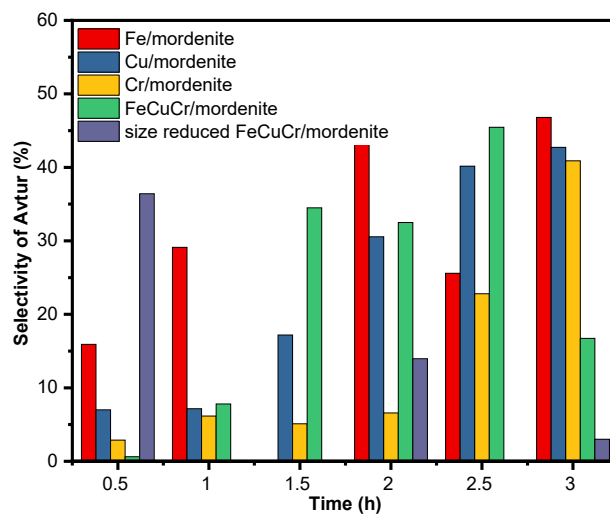


Fig 6. Comparison of the selectivity of the results of the aviation fuel from the reaction of cracking using the 5 variations of the catalyst

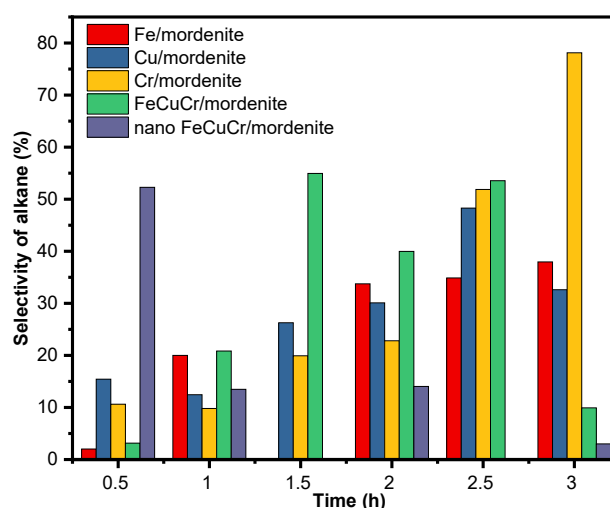


Fig 7. Comparison of the selectivity of alkanes from the reaction of cracking using the 5 variations of the catalyst

revealed that Cr/mordenite catalysts resulted in superior alkane conversion when compared to the remaining catalysts for reaction done for 3 h. All the data obtained suggest that the metals under study could influence the catalytic nature of mordenite in stearic acid conversions. Moreover, by using the metal combined catalyst, stearic acid's selectivity to produce aviation fuel was less effective at the initial reaction time but reached optimum after 2 h (up to 55.2%). Similarly, optimum alkane conversion was reached at 1.5 h (up to 54.9%). Although the conversion could not reach a desirable

optimum condition for Fe/mordenite catalyst (in terms of its selectivity towards alkane conversion) and Cr/mordenite catalyst (in terms of its selectivity towards aviation fuel conversion), however, it could be seen that FeCuCr/mordenite showed stable and selective performance (on both aviation fuel and alkane) as the reaction process reached 1.5 h. As could be seen from the above findings, the addition of metals to Mordenite could affect its selectivity. Also, the combination of the three metals affects the catalytic nature of the Mordenite. Therefore, it could be assumed that the catalytic process of mordenite could be enhanced by the addition of metal ions. Moreover, subsequent evaluation on using size-reduced FeCuCr/mordenite opens the possibility of a new way in catalytic processes. From Fig. 6 and 7, it can be observed that smaller particles of the FeCuCr/mordenite tend to have higher selectivity of aviation fuel and alkane on initial time reaction. This indicates that the nano FeCuCr/mordenite catalysts were active at the initial reaction time, however, became deactivated as the reaction took longer than 0.5 h. This statement is also supported by conversion data of all modified catalysts (Fig. 8). Components of BAF produced from FeCuCr/mordenite conversion include xylene, mesitylene, dodecane, tridecane, tetradecane, and pentadecane. Constituents of BAF produced by nano FeCuCr/mordenite catalyst include benzene, tetradecane, and pentadecane. While all of the catalysts increased the percentage of stearic acid conversion over time, the size reduced performed optimum conversion at the initial time (100% conversion at 0.5 h). Reducing the size of the catalyst caused an increase in the active sites. The increasing effectivity was common and be main reason application of nanotechnology in many fields, including the catalytic process [27-29]. As such, the cracking

process was more efficient, leading to a higher percentage of selective production of BAF.

In addition to determining the composition, fuel specifications and performance requirements are also needed (Table 2). The specifications required for aircraft fuel are (1) maximum permissible viscosity, (2) maximum pour point, (3) cloud point, (4) minimum allowable flashpoint, and (5) maximum amount of sulfur. The results showed that the kinetic viscosity of 0.46 cSt was smaller than the characteristic viscosity at 40 °C for aircraft fuel according to ASTM of 1.6–7 cSt. Pour point values, total sulfur, and ash (< -30 °C, 0.08%, 0.004%) have characteristics for aircraft fuel according to ASTM of a maximum of 15 °C, 1%, and 0.01%, respectively. The compound produced from this cracking reaction burns at room temperature. According to ASTM, the minimum flash point tolerance is 38 °C. The cloud point obtained is very low (< -30 °C). This is a necessary condition for fuel performance because the lower the temperature,

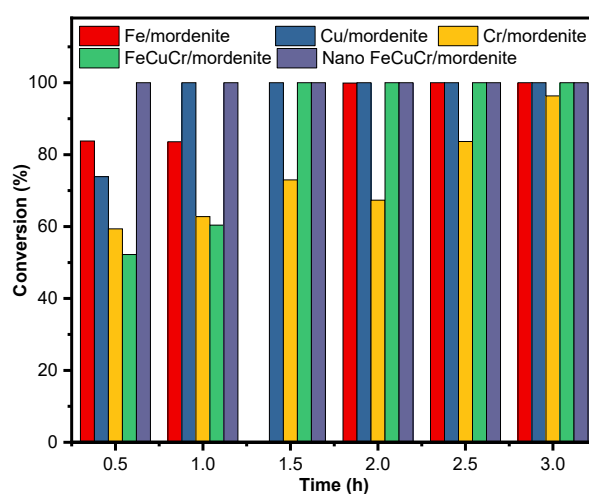


Fig 8. Comparison of the conversion of the reaction cracking with stearic acid using 5 variations of the catalyst

Table 2. Specifications for the obtained aviation-fuel

Type of test	Result	Unit	Test method
Kinematic viscosity (40 °C)	0.46	cSt	ASTM D 445-97
Pour point	< -30	°C	ASTM D 97-85
Cloud point	< -30	°C	ASTM D 2500
Flash point	burns at room temperature (around 25)	°C	ASTM D 93-00
Sulfur content	0.08	%	SNI 7431:2015
Ash content	0.004	%	ASTM D 482

the longer the liquid fuel solidifies, so it is not easy to clog the filter and fuel injectors in the engine.

■ CONCLUSION

The present study successfully reveals the impregnation of Fe, Cu, and Cr onto mordenite through several characterizations. The modified catalyst performs good stearic acid cracking, even with single metal and combined metal impregnation. The size modification on the catalyst helps very well in increasing acid sites upon the catalyst. The cracking reaction changes stearic acid into several compounds, including alkanes, alkenes, alcohols, ketones, cycloalkanes, and benzene containing aviation fuel components. It also shows that Fe/mordenite, Cu/mordenite, Cr/mordenite, and FeCuCr/mordenite have optimum catalytic activity mostly over a 1.5 h reaction. At the same time, the size reduced FeCuCr/mordenite showed good activity at the initial reaction. Selective production of BAF compound in the present study reached up to 30.27% by using FeCuCr/mordenite catalyst. The BAF constituents included xylene, mesitylene, dodecane, tridecane, tetradecane, and pentadecane. On the other hand, 19.85% selectivity was obtained when nano FeCuCr/mordenite catalyst was used to produce BAF, which contains benzene, tetradecane, and pentadecane.

■ ACKNOWLEDGMENTS

The authors thank the Ministry of Research, Technology, and Higher Education, Republic Indonesia, for financial support and Universitas Airlangga through PUF research funding under contract 1900/UN 3.1.8/LT/2018.

■ REFERENCES

- [1] Blakey, S., Rye, L., and Wilson, C.W., 2011, Aviation gas turbine alternative fuels: A review, *Proc. Combust. Inst.*, 33 (2), 2863–2885.
- [2] Sabarman, J.S., Legowo, E.H., Widiputri, D.I., and Siregar, A.R., 2019, Bioavtur synthesis from palm fatty acid distillate through hydrotreating and hydrocracking processes, *Indones. J. Energy*, 2 (2), 99–110.
- [3] Zanata, M., Amelia, S.T.W., Mumtazy, M.R., Kurniawansyah, F., and Roesyadi, A., 2019, Synthesis of bio jet fuel from crude palm oil by HEFA (Hydroprocessed Esters and Fatty Acids) using Ni-Mo catalyst supported by rice husk ash-based SiO₂, *Mater. Sci. Forum*, 964, 193–198.
- [4] Carli, M.F., Susanto, B.H., and Habibie, T.K., 2018, Synthesis of bioavtur through hydrodeoxygenation and catalytic cracking from oleic acid using NiMo/zeolite Catalyst, *E3S Web Conf.*, 67, 02023.
- [5] Abdulloh, A., Purkan, P., and Hardiansyah, N., 2017, Reparasi dan karakterisasi alfa-Fe₂O₃/zeolit Y untuk reaksi perengkahan asam palmitat, *Jurnal Kimia Riset*, 2 (2), 69–76.
- [6] Abdulloh, A., Widati A.A., and Tamamy F., 2016, Hidrolisis minyak jarak pagar menjadi asam lemah bebas menggunakan katalis CaO, *Jurnal Kimia Riset*, 1 (1), 1–6.
- [7] Saxena, S.K., and Viswanadham, N., 2017, Enhanced catalytic properties of mesoporous mordenite for benzylation of benzene with benzyl alcohol, *Appl. Surf. Sci.*, 392, 384–390.
- [8] Chai, M., Liu, R., and He, Y., 2020, Effects of SiO₂/Al₂O₃ ratio and Fe loading rate of Fe-modified ZSM-5 on selection of aromatics and kinetics of corn stalk catalytic pyrolysis, *Fuel Process. Technol.*, 206, 106458.
- [9] Bahadi, M.A., Japir, A.W., Salih, N., and Salimon, J., 2016, Free fatty acids separation from Malaysian high free fatty acid crude palm oil using molecular distillation, *Malays. J. Anal. Sci.*, 20 (5), 1042-1051.
- [10] Tuminah, S., 2010, Efek perbedaan sumber dan struktur kimia asam lemak jenuh terhadap kesehatan, *Bul. Penelit. Kesehat.*, 38 (1), 43–51.
- [11] Widiyanto, W., Suranto, S., Kusumanti, E., and Mulyono, M., 2016, The influence of protected kapok seed oil supplementation on in vitro ruminal fermentability and linoleic acid status with Etawah crossbred goat rumen fluid and elephant grass as feed, *Afr. J. Agric. Res.*, 11 (14), 1237–1244.
- [12] Chaikul, P., Lourith, N., and Kanlayavattanukul, M., 2017, Antimelanogenesis and cellular antioxidant

- activities of rubber (*Hevea brasiliensis*) seed oil for cosmetics, *Ind. Crops Prod.*, 108, 56–62.
- [13] Srinivasan, G.R., and Jambulingam, R., 2018, Comprehensive study on biodiesel produced from waste animal fats-A review, *J. Environ. Sci. Technol.*, 11 (3), 157–166.
- [14] Purandaradas, A., Silambarasan, T., Murugan, K., Babujanarthanam, R., Gandhi, A.D., Dhandapani, K.V., Anbumani, D., and Kavitha, P., 2018, Development and quantification of biodiesel production from chicken feather meal as a cost-effective feedstock by using green technology, *Biochem. Biophys. Rep.*, 14, 133–139.
- [15] Permata, M.L., and Trisunaryanti, W., 2020, The effect of nickel content impregnated on zeolite toward catalytic activity and selectivity for hydrotreating of cashew nut shell liquid oil, *Rasayan J. Chem.*, 13 (1), 772–779.
- [16] Weng, Y., Qiu, S., Ma, L., Liu, Q., Ding, M., Zhang, Q., Zhang, Q., and Wang, T., 2015, Jet-fuel range hydrocarbons from biomass-derived sorbitol over Ni-HZSM-5/SBA-15 catalyst, *Catalysts*, 5 (4), 2147–2160.
- [17] Zhao, Y., Liu, J., Xiong, G., and Guo, H., 2017, Enhancing hydrothermal stability of nanosized HZSM-5 zeolite by phosphorus modification for olefin catalytic cracking of full-range FCC gasoline, *Chin. J. Catal.*, 38 (1), 138–145.
- [18] Liang, J., Zhang, Z., Wu, K., Shi, Y., Pu, W., Yang, M., and Wu, Y., 2019, Improved conversion of stearic acid to diesel-like hydrocarbons by carbon nanotubes-supported CuCo catalysts, *Fuel Process. Technol.*, 188, 153–163.
- [19] Zhang, X., Zhong, J., Wang, J., Zhang, L., Gao, J., Liu, A., 2009, Catalytic performance and characterization of Ni-doped HZSM-5 catalysts for selective trimerization of *n*-butene, *Fuel Process. Technol.*, 90 (7-8), 863–870.
- [20] Li, J., Tong, Z., Xi, Y., Hu, Z., and Zhu, Z., 2016, Highly-efficient conversion of methanol to *p*-xylene over shape-selective Mg-Zn-Si-HZSM-5 catalyst with fine modification of pore-opening and acidic properties, *Catal. Sci. Technol.*, 6 (13), 4802–4813.
- [21] Zambare A.S., Ou, J., Wong, D.S.H., Yao, C.W., and Jang, S.S., 2019, Controlling the product selectivity in the conversion of methanol to the feedstock for phenol production, *RSC Adv.*, 9 (41), 23864–23875.
- [22] Fani, K., Lycourghiotis, S., Bourikas, K., and Kordouli, E., 2021, Biodiesel upgrading to renewable diesel over nickel supported on natural mordenite catalysts, *Ind. Eng. Chem. Res.*, 60 (51), 18695–18706.
- [23] Anderson, J.A., 2011, *Supported Metals in Catalysis*, 2nd Ed., Imperial College Press, London, UK.
- [24] Jia, Y., Wang, J., Zhang, K., Feng, W., Liu, S., Ding, C., and Liu, P., 2017, Nanocrystallite self-assembled hierarchical ZSM-5 zeolite microsphere for methanol to aromatics, *Microporous Mesoporous Mater.*, 247, 103–115.
- [25] Stuart, B., 2004, *Infrared Spectroscopy: Fundamentals and Applications*, John Wiley & Sons Inc., Chichester, UK.
- [26] Narayan, S., Vijaya, J.J., Sivasanker, S., Alam, M., Tamizhdurai, P., and Kennedy, L.J., 2015, Characterization and catalytic reactivity of mordenite – Investigation of selective oxidation of benzyl alcohol, *Polyhedron*, 89, 289–296.
- [27] Girma, W.M., Fahmi, M.Z., Permadi, A., Abate, M.A., and Chang, J.Y., 2017, Synthetic strategies and biomedical applications of I–III–VI ternary quantum dots, *J. Mater. Chem. B*, 5 (31), 6193–6216.
- [28] Aung, Y.Y., Wibrianto, A., Sianturi, J.S., Ulfa, D.K., Sakti, S.C., Irzaman, I., Yulianto, B., Chang, J.Y., Kwee, Y., and Fahmi, M.Z., 2021, Comparison direct synthesis of hyaluronic acid-based carbon nanodots as dual active targeting and imaging of HeLa cancer cells, *ACS Omega*, 6 (20), 13300–13309.
- [29] Fahmi, M.Z., and Chang, J.Y., 2014, A facile strategy to enable nanoparticles for simultaneous phase transfer, folate receptor targeting, and cisplatin delivery, *RSC Adv.*, 4 (100), 56713–56721.